J Mol Neurosci (2012) 48:111–126
DOI 10.1007/s12031-012-9783-8

Neuroglial Expression of the MHCI Pathway and PirB Receptor Is Upregulated in the Hippocampus with Advanced Aging

Heather D. VanGuilder Starkey · Colleen A. Van Kirk · Georgina V. Bixler · Caesar G. Imperio · Vijay P. Kale · Jacob M. Serfass · Julie A. Farley · Han Yan · Junie P. Warrington · Song Han · Matthew Mitschelen · William E. Sonntag · Willard M. Freeman

Received: 7 March 2012 / Accepted: 16 April 2012 / Published online: 6 May 2012
© Springer Science+Business Media, LLC 2012

Abstract The hippocampus undergoes changes with aging that impact neuronal function, such as synapse loss and altered neurotransmitter release. Nearly half of the aged population also develops deficits in spatial learning and memory. To identify age-related hippocampal changes that may contribute to cognitive decline, transcriptomic analysis of synaptosome preparations from adult (12 months) and aged (28 months) Fischer 344–Brown Norway rats assessed for spatial learning and memory was performed. Bioinformatic analysis identified the MHCI pathway as significantly upregulated with aging. Age-related increases in mRNAs encoding the MHCI genes RT1-A1, RT1-A2, and RT1-A3 were confirmed by qPCR in synaptosomes and in CA1 and CA3 dissections. Elevated levels of the MHCI cofactor (B2m), antigen-loading components (Tap1, Tap2, Tapbp), and two known MHCI receptors (PirB, Klra2) were also confirmed. Protein expression of MHCI was elevated with aging in synaptosomes, CA1, and DG, while PirB protein expression was induced in both CA1 and DG. MHCI expression was localized to microglia and neuronal excitatory postsynaptic densities, and PirB was localized to neuronal somata, axons, and dendrites. Induction of the MHCI antigen processing and presentation pathway in hippocampal neurons and glia may contribute to age-related hippocampal dysfunction by increasing neuroimmune signaling or altering synaptic homeostasis.

Keywords Aging · Hippocampus · Major histocompatibility complex I · Paired immunoglobulin-like receptor B · Synapse · Neuroimmune

Electronic supplementary material The online version of this article (doi:10.1007/s12031-012-9783-8) contains supplementary material, which is available to authorized users.

H. D. V. Starkey · C. A. Van Kirk · G. V. Bixler · C. G. Imperio · V. P. Kale · J. M. Serfass · W. M. Freeman (✉)
Department of Pharmacology, Penn State College of Medicine, 500 University Drive, R130, Hershey, PA 17033, USA
e-mail: wfreeman@psu.edu

J. A. Farley · H. Yan · J. P. Warrington · S. Han · M. Mitschelen · W. E. Sonntag
Reynolds Oklahoma Center on Aging, Donald W. Reynolds Department of Geriatric Medicine, University of Oklahoma Health Sciences Center, Oklahoma City, OK, USA

Introduction

Declining hippocampal function is associated with advanced aging and leads to impaired cognitive function in nearly half of the population over 60 years of age (Small 2002; Hedden and Gabrieli 2004). The detrimental effects of aging on cognitive functions such as spatial learning and memory reduce quality of life and independence of older individuals (Tomaszewski et al. 2009; Fiocco and Yaffe 2010). With a growing aged population, it is necessary to delineate the age-related neurobiological changes that may contribute to hippocampal dysfunction and to identify target processes/pathways for therapeutic interventions to maintain or restore hippocampal function.

Normative hippocampal aging occurs in the absence of overt pathological abnormalities and is associated with

synapse loss rather than neuron death (Shi et al. 2005; Shamy et al. 2006; Long et al. 2009; Hara et al. 2011). Additionally, electrophysiological and molecular correlates of synaptic plasticity are disrupted in the hippocampus with advanced aging and may underlie age-related deficits of cognitive function (Barnes 1979, 2003). Multiple cellular processes including increased inflammation and oxidative stress, protein misfolding/accumulation, and synaptic dysfunction (VanGuilder and Freeman 2011) likely exert an additive insult that contributes to the increased neuroimmune activation characteristic of hippocampal aging (Lucin and Wyss-Coray 2009; VanGuilder et al. 2011a).

Recent discoveries have identified novel mechanisms through which neuroimmune signaling and neuron–glia interactions can regulate synaptic plasticity, neurotransmission, and ultimately behavior, providing a potential link between increased hippocampal glial activation, inflammation response, and age-related hippocampal dysfunction. For example, microglia not only clear cellular/synaptic debris, but also actively participate in synapse pruning (Paolicelli et al. 2011) and provide feedback regulation of synapse function (Roumier et al. 2004). Microglial activation increases in the hippocampus with aging (Ogura et al. 1994; Gavilan et al. 2007; VanGuilder et al. 2011a) and may contribute to hippocampal dysfunction by altering regulation of neuronal activity and structure (Yirmiya and Goshen 2011). Using the rat model employed in the present study, we have previously demonstrated that age-related activation of hippocampal microglia is associated with upregulation of the MHCII immune response pathway (VanGuilder et al. 2011a). In the present study of hippocampal aging, we examined the expression of a recently described neuroimmune signaling mechanism, the MHCI antigen processing and presentation pathway. Unlike MHCII, MHCI pathway components are expressed by neurons as well as microglia and modulate synapse formation and function (Boulanger 2009). Here, we describe transcript level upregulation of MHCI antigen processing and presentation machinery and the associated PirB receptor, as well as protein level upregulation of both MHCI and PirB, in the hippocampus with advanced aging. The age-related increases in expression of MHCI pathway components occurred regardless of deficits of hippocampus-dependent spatial learning and memory, as assessed by Morris water maze testing of adult and aged rats. MHCI protein expression was localized to microglia and neuronal somata and postsynaptic densities, while PirB was restricted to neuronal cell bodies and processes. Given the emerging roles of MHCI and PirB as regulators of neuronal structure and function, increased MHCI signaling, while not directly associated with behavioral deficits in this study, may contribute to the age-related electrophysiological disruptions and synapse loss characteristic of the aged hippocampus.

Materials and Methods

Animals

Male Fischer 344 × Brown Norway (F1) hybrid rats (see Table 1 for cohort information) were purchased from the National Institute on Aging colony at Harlan Industries (Indianapolis, IN, USA) as previously described (VanGuilder et al. 2011a, b, 2012). Mature adult (middle-aged, 12 months) and aged (26–28 months) rats were used in all animal studies. Rats were singly housed in laminar flow cages with free access to food and water (Purina Mills, Richmond, IN, USA) in the OUHSC specific pathogen-free barrier facility, which maintains a 12-h light/dark cycle and constant temperature and humidity. One week following completion of behavioral testing, rats were sacrificed by decapitation without anesthesia, and the hippocampi rapidly dissected for preparation of synaptosomes (cohort 1) or dissection of specific hippocampal subregions (cohort 2). For immunohistochemical localization experiments, aged rats were perfusion-fixed, and their brains extracted for immunohistochemical localization experiments (cohort 3) (Table 1). All animals were examined for exclusionary criteria (e.g., frank kidney disease, cardiac hypertrophy, peripheral tumors, pituitary tumors, cortical atrophy). The OUHSC animal facilities are fully accredited by the Association for Assessment and Accreditation of Laboratory Animal Care, and all animal procedures were approved by the Institutional Animal Care and Use Committee in compliance with the Public Health Service Policy on Humane Care and Use of Laboratory Animals and the National Research Council's Guide for the Care and Use of Laboratory Animals.

Morris Water Maze Testing

Cognitive assessment was performed using a variation of the Morris water maze, and the behavioral stratification of the cohorts included in the present study has been described in full previously (VanGuilder et al. 2011a, b, 2012). Briefly, a maze pool (1.7 m in diameter, 0.6 m in height) was filled to a depth of 25 cm with water made opaque with non-toxic water-based white food coloring, and a retractable 12-cm escape platform was fixed 2 cm beneath the water's surface. Visual cues, serving as reference cues for the escape platform location, were fixed to a curtain surrounding the maze pool. Maze performance was recorded by a center-mounted camera and analyzed by an automated tracking system (Noldus Ethovision XT, Wageningen, Netherlands). Task acquisition was conducted in four blocks of five 60-s trials, each performed over 2 days, with the escape platform located in the same position throughout training, and with start positions pseudo-randomized. A 30-s probe trial was performed after each acquisition block, with the escape platform retracted

Table 1 Animal cohort information

Cohort	Age (months)	Group	Number	Mean proximity to platform location (cm)	Sample type	Analyses performed
1[a]	12	Adult	5	48±1.9	Hippocampal synaptosomes	Morris water maze testing, transcriptomic analysis, qPCR, immunoblotting
	28	Aged intact	8	52±2.4		
	28	Aged impaired	7	68±1.6		
2[b]	12	Adult	7	49±1.1	Hippocampal subregions (CA1, CA3, DG)	Morris water maze testing, qPCR, immunoblotting
	26	Aged intact	7	48±1.4		
	26	Aged impaired	10	59±1.4		
3	26	Aged	3	N/A	Perfusion-fixed sagittal brain sections	Immunohistochemistry

[a] Previously described in VanGuilder et al. (2011a)

[b] Previously described in VanGuilder et al. (2011b)

to the bottom of the tank. To avoid extinguishing memory of the platform location, the platform was then raised and rats were given 60 s to locate the platform using the surrounding cues. Mean proximity to the escape platform location during probe trials was used to segregate aged animals into cognitively intact and impaired groups relative to adult group performance, allowing retrospective analysis of acquisition phase data (path length to the platform) by group. Aged rats were classified as cognitively intact if their average probe trial performance (i.e., mean proximity to platform location across four probe trials) was within the range of the adult group. Aged rats with mean proximity values greater than two standard deviations above the adult group mean were classified as cognitively impaired. Differential probe trial performance between groups was verified by one-way ANOVA with Student–Newman–Keuls (SNK) post hoc testing. One week after completion of maze testing, animals were sacrificed and their brains dissected for hippocampal synaptosome isolation (cohort 1) or subregion dissection (cohort 2).

Hippocampal Synaptosome Preparation

Hippocampal synaptosomes were prepared as previously described (VanGuilder et al. 2010, 2011b). Immediately following sacrifice, individual hippocampi from each rat were rapidly dissected and homogenized in ice-cold buffered sucrose (320 mM sucrose, 4 mM HEPES, 1 mM Na_3VO_4, pH 7.4). Homogenates were centrifuged to pellet nuclear/cytoskeletal fractions (nuc/cyt; 12 min, 1,000×*g*, 4°C). The resulting supernatants were then centrifuged to pellet the synaptosomal fractions (syn; 16 min, 25,000×*g*, 4°C). Synaptosomal fractions were washed by resuspending in 5 mL buffered sucrose and centrifuging to re-pellet samples (16 min, 25,000×*g*, 4°C).

Synaptosome Quality Assessment

To demonstrate depletion of nuclear contaminants, whole hippocampus, nuclear/cytoskeletal fractions, and synaptosome-containing fractions were immunoblotted for histone 4. Enrichment of presynaptic and postsynaptic compartments was assessed by immunoblotting for synaptophysin and PSD-95, respectively. Since glial components are frequently identified in synaptosomal preparations (Chicurel et al. 1993; Gylys et al. 2000; VanGuilder et al. 2010), inclusion of astrocyte- and microglia-derived material was evaluated by immunoblotting for glial fibrillary acidic protein (GFAP) and ionized calcium binding adaptor molecule 1 (Iba1). Immunoblot methods are described below, and antibodies are described in Table 2.

Visual examination of synaptosome preparations by electron microscopy was also performed. Immediately following preparation, pelleted synaptosome-containing fractions were fixed for 3 h at room temperature in 0.1 M sodium cacodylate-buffered gluteraldehyde (2.5 %) and paraformaldehyde (2 %) with 0.05 % $CaCl_2$, pH 7.3. Pellets were washed with 0.1 M sodium cacodylate buffer and were post-fixed overnight at 4°C with osmium tetroxide (1 %) and potassium ferrocyanide (1.5 %) in 0.1 M sodium cacodylate buffer. Samples were then dehydrated in graded ethanol and propylene oxide and incubated overnight at room temperature in 1:1 propylene oxide/Epon 812 resin. Resin-infiltrated synaptosome pellets were rotated twice into fresh 100 % Epon 812 resin at 12-h intervals prior to embedding in 100 % Epon and polymerizing for 3 days at 60°C. Ultrathin sections were generated using a Sorvall MT2-B microtome, mounted on round copper mesh grids, and stained with 2 % uranyl acetate and 0.4 % lead citrate in the Penn State College of Medicine Electron Microscopy Laboratory. Sections were imaged with a JEOL JEM1400 digital capture transmission electron microscope.

Hippocampal Subregion Dissection

For dissection of individual subregions, each hippocampus was hemisected and the dorsomedial portion was further dissected into four blocks perpendicular to the longitudinal axis. From these blocks, the CA3 was dissected by cutting

Table 2 Antibody information

Antibody	Supplier	Catalog #	Host	Use	Method
GFAP	Abcam	AB7260	Rabbit	Primary	IHC
Histone 4	Cell Signaling Technology	2592	Rabbit	Primary	IB
Iba1	Wako	01919741	Rabbit	Primary	IHC
Iba1	Wako	01620001	Rabbit	Primary	IB
MAP2	Cell Signaling Technology	4542	Rabbit	Primary	IHC
MHCI/RT1A (Ox-18)	BD Pharmingen	554917	Mouse	Primary	IB/IHC
Neurofilament heavy chain	Sigma Aldrich	N0142	Mouse	Primary	IHC
PirB/Lilrb3 (A-20)	Santa Cruz Biotechnology	SC9608	Goat	Primary	IB/IHC
PSD95	Abcam	AB18258	Rabbit	Primary	IHC
Synapsin 1	Abcam	AB8-10	Rabbit	Primary	IHC
Synaptophysin	Sigma	S5768	Mouse	Primary	IB
Anti-goat [F(ab′)$_2$] DL549	Jackson ImmunoResearch	705506147	Donkey	Secondary	IHC
Anti-goat IgG (HRP-conjugated)	Santa Cruz Biotechnology	SC2768	Rabbit	Secondary	IB
Anti-mouse [F(ab′)$_2$] DL488	Jackson ImmunoResearch	715486150	Donkey	Secondary	IHC
Anti-mouse IgG (HRP-conjugated)	Thermo Scientific	32430	Goat	Secondary	IB
Anti-rabbit [F(ab′)$_2$] DL649	Jackson ImmunoResearch	711496152	Donkey	Secondary	IHC
Anti-rabbit IgG (HRP-conjugated)	GE Healthcare	NA934V	Donkey	Secondary	IB

IHC immunohistochemistry, *IB* immunoblotting

along the edge of the DG and the CA1 and DG were dissected by cutting along the hippocampal fissure as described previously (VanGuilder et al. 2011a).

RNA Isolation

RNA was isolated and purified from hippocampal synaptosome and subregion (CA1, CA3, DG) samples using TRI-Reagent/BCP/isopropanol extraction as previously described (VanGuilder et al. 2011a). RNA was assessed for quantity and quality by spectrometry (NanoDrop ND1000; Thermo Scientific, Wilmington, DE, USA) and microfluidic chips (Agilent 2100 Expert Bioanalyzer Nano Chip, Agilent, Palo Alto, CA, USA). Only samples with an RNA integrity number (RIN) >8 were included in whole genome transcriptomic and qPCR analyses.

Whole Genome Gene Expression Analysis

Transcriptomic analysis of hippocampal synaptosomes isolated from adult, aged intact, and aged impaired rats (cohort 1, n=5–7/group, see Table 1 for cohort information) was performed in the Penn State College of Medicine Genome Sciences Facility using Illumina RatRef-12 microarrays (Illumina, San Diego, CA, USA) as previously described (VanGuilder et al. 2011a). Briefly, first-strand cDNA was reverse-transcribed from 500 ng RNA by incubating for 2 h at 42°C with T7 Oligo(dT) primers, 10× First-Strand buffer, dNTPs, RNase inhibitor, and ArrayScript (Illimina). Second-strand cDNA was synthesized by incubating for 2 h at 16°C with 10× Second-Strand buffer, dNTPs, DNA polymerase, and RNase H. Second-strand cDNA was then purified using the Illumina TotalPrep kit (Ambion, Foster City, CA, USA) and eluted with 55°C nuclease-free water. cRNA was synthesized from second-strand cDNA using the MEGAscript kit (Ambion) and biotinylated by incubating for 14 h at 37°C with T7 10× reaction buffer, T7 Enzyme mix, and Biotin-NTP mix. Labeled cRNA was purified with the Illumina TotalPrep RNA Amplification kit (Ambion) and quantitated by spectrometry (NanoDrop ND1000, Thermo Scientific). Labeled cRNA (750 ng) was hybridized to RatRef-12 BeadChip microarrays for 20 h at 58°C. BeadChips were then washed and streptavadin-Cy3-stained, dried by centrifuging at 275×g, and scanned and digitized using a Bead Station Bead Array Reader.

Arrays were quality control checked, and data were initially analyzed using average normalization with background subtraction performed with GenomeStudio software (Illumina). The full microarray dataset is available in the Gene Expression Omnibus, accession# (GSE29511). Flat files were imported into GeneSpring GX11 (Agilent) software for data analysis. Probes were filtered to include only those with "present" or "marginal" calls in 100 % of samples in at least one of three experimental groups, as determined by detection of p values generated by GenomeStudio. Statistically significant differential gene expression was determined using a combination of pair-wise absolute value fold change cutoff of 1.2 and one-way ANOVA with SNK post hoc tests $p<0.05$ (VanGuilder et al. 2011a), for which a median false discovery rate (FDR) (Benjamini et al. 2001) was calculated. The

distribution of differential gene expression was visualized by a heatmap generated in GeneSpring GX11, with hierarchical clustering by conditions and genes using Euclidean distance and complete linkage. Gene ontology (GO) classifications were determined from differentially expressed genes using GeneSpring GX11, and pathway analysis was performed using Ingenuity Pathway Analysis software (Ingenuity Systems, Redwood City, CA, USA).

RT-qPCR

To confirm differential expression of target mRNAs, qPCR analysis of hippocampal synaptosomes as well as dissected hippocampal subregions was performed (cohorts 1 and 2, see Table 1 for cohort information). cDNA was reverse-transcribed from RNA using the High Capacity cDNA Reverse Transcription kit (Applied Biosystems, Foster City, CA, USA) with random priming as previously described (VanGuilder et al. 2011a). qPCR-based target mRNA quantitation was performed using TaqMan Assay-On-Demand gene-specific primer/probe assays (Table 3) and a 7900HT Sequence Detection System (Applied Biosystems). Relative gene expression was calculated using the $2^{-\Delta\Delta Ct}$ analysis method with β-actin as the endogenous control. Data were statistically analyzed by two-tailed *t* tests for comparison of adult and aged groups, and for three-group comparisons of adult, aged intact, and aged impaired by one-way ANOVA with SNK post hoc testing. To control for multiple testing type I error, *t* tests and ANOVAs were subjected to a Benjamini Hochberg multiple testing correction to adjust the critical value based on the number of tests performed (Narum 2006).

Protein Isolation

Synaptosome samples and hippocampal subregion dissections were homogenized by bead mill in a detergent-based protein lysis buffer containing protease and phosphatase inhibitors (100 mM NaCl, 20 mM HEPES, 1 mM EDTA, 1 mM dithiothreitol, 1.0 % Tween20, 1 mM Na_3VO_4, 1 Complete Mini EDTA-Free Protease Inhibitor Cocktail Tablet (Roche Applied Science, Indianapolis, IN, USA) for every 10 mL lysis buffer). Lysates were incubated for 15 min at 4°C with gentle rocking, insoluble protein was pelleted by centrifugation (12 min, 10,000×*g*, 4°C), and the soluble protein-containing supernatant was stored at −80°C for subsequent experimentation. Protein yields were determined by bicinchoninic acid quantitation (Pierce, Rockford, IL, USA) in technical triplicates, and samples were adjusted to a concentration of 1 μg/μL in protein lysis buffer and LDS sample buffer (Invitrogen, Carlsbad, CA, USA).

Immunoblotting

Immunoblotting was performed and normalized to Deep Purple total protein staining as described previously (VanGuilder et al. 2011b, 2012). Samples were denatured at 95°C for 5 min, 10 μg protein per sample was separated by SDS-PAGE using Criterion precast Tris–HCl 4–20 % acrylamide gradient gels (BioRad, Hercules, CA, USA) and proteins were transferred to PVDF membranes (HyBond-P, GE Healthcare, Piscataway, NJ, USA). Membranes were blocked with 5 % nonfat milk or 3 % BSA in PBS with 1.0 % Tween-20 (PBST), incubated overnight with primary antibodies (Table 2) in blocking solution, washed with PBST, and incubated with horseradish peroxidase-conjugated, affinity-purified secondary antibodies. After washing, membranes were developed with enhanced chemiluminescence substrate (Pierce) and visualized on film (CL-X Posure, Thermo Scientific). Films were digitized at a resolution of 600 d.p.i., and immunoreactive bands were quantitated using semi-automated digital densitometry software (ImageQuant TL, GE Healthcare). For each sample and target protein, data were normalized to whole-lane total protein densitometry, scaled to

Table 3 Primer/probe sets used in qPCR confirmation studies

Gene symbol	Gene ID number	Gene name	Gene expression assay catalogue #
B2m	24223	Beta-2 microglobulin	Rn00560865
Klra2 (Ly49)	494194	Killer cell lectin-like receptor, subfamily A, member 2	Rn02346797
PirB (Lilrb3)	65146	Leukocyte immunoglobulin-like receptor, subfamily B (with TM and ITIM domains), member 3	Rn00581823
RT1-A1	24973	RT1 class Ia, locus A1	Rn02749313
RT1-A2	24974	RT1 class Ia, locus A2	Rn03021105
RT1-A3	309627	RT1 class I, locus A3	Rn02346174
Tap1	24811	Transporter 1, ATP-binding cassette, sub-family B (MDR/TAP)	Rn00709612
Tap2	24812	Transporter 2, ATP-binding cassette, sub-family B (MDR/TAP)	Rn00583182
Tapbp	25217	TAP binding protein	Rn00583606

mean adult values, and statistically analyzed by two-tailed *t* test (all aged vs. adult comparisons) and one-way ANOVA with SNK post hoc testing (three-group comparisons).

Immunohistochemistry

To assess the localization of upregulated MHCI and PirB protein in the aged hippocampus, aged rats (26 months; cohort 3, see Table 1 for cohort information) were anesthetized with ketamine/xylazine and transcardially perfused with 6 U/mL heparin (sodium salt) in PBS followed by phosphate-buffered 4 % paraformaldehyde (pH 7.4) as described previously (VanGuilder et al. 2012). Brains were hemisected sagittally along the central sulcus, immersion-fixed in 4 % paraformaldehyde (pH 7.4) overnight at 4°C, rinsed with PBS, cryoprotected with 30 % sucrose, and embedded in Tissue-Tek cryosectioning medium (OCT; Sakura Finetek, Torrance, CA, USA). Twelve-micrometer sagittal cryosections were postfixed with 2.0 % paraformaldehyde, pH 7.4, blocked with 10 % donkey serum (Jackson ImmunoResearch, West Grove, PA, USA) in 0.1 % Triton X-100/PBS, and incubated with primary antibodies (Table 2) in blocking solution overnight at 4°C. Sections were washed with 0.1 % Triton X-100/PBS, incubated with affinity-purified, species-appropriate fluorescence-conjugated secondary antibodies (Table 2) diluted in blocking solution, and counterstained with Hoechst 33258 (5 μg/mL, Invitrogen, Carlsbad, CA, USA). After washing, slides were coverslipped with Aqua Poly/mount (Polysciences, Warrington, PA, USA) and imaged by confocal microscopy (Leica TCS SP2 AOBS, Exton, PA, USA). High-resolution images of cells/features of interest were acquired using a×63 objective with×4 digital zoom and are presented as single optical sections. Broad-field images of hippocampi were acquired with a Nikon TE2000-E inverted epi-fluorescent microscope. Noise reduction and background subtraction were performed using Adobe Photoshop CS4 software (Adobe Systems, San Jose, CA, USA).

Results

Behavioral Stratification of Adult and Aged Rats Using the Morris Water Maze

Hippocampus-dependent cognitive performance of two cohorts of adult (12 months) and aged (26–28 months) male Fischer 344×Brown Norway hybrid rats was assessed by Morris water maze and has been described in full previously (VanGuilder et al. 2011a, b, 2012) (see Table 1 for cohort information). Behavioral stratification data are summarized in Table 1 to facilitate group-based comparison of gene/protein expression in adult, aged cognitively intact, and aged cognitively impaired rats. Aged rats were assigned to cognitively intact or impaired categories relative to adult rats based on mean proximity to the escape platform location in probe trials, as previously described (VanGuilder et al. 2011a, b, 2012). There were no significant differences in swim velocity, path length to a visible platform, or total distance swum, nor were the weights of aged intact and aged impaired rats statistically different.

Quality Assessment of Hippocampal Synaptosome Preparations

Hippocampal synaptosome preparations were evaluated by electron microscopy and immunoblotting. Microscopic analysis of synaptosome-containing fractions revealed intact synaptosomes comprised of vesicle-containing presynaptic elements adjacent to postsynaptic terminals with visible postsynaptic densities (Fig. 1a, top). In agreement with previous findings (VanGuilder et al. 2010), there were no significant group differences in total detergent-soluble protein yields between adult, aged intact, and aged impaired rats. Immunoblot analysis was performed to assess the biochemical composition of synaptosome preparations (syn) compared to hippocampal homogenates (hipp) and nuclear/cytoskeletal fractions (nuc/cyt) (Fig. 1a, bottom). In agreement with electron microscopic visualization, synaptosome fractions were depleted of the nuclear marker histone 4, which was enriched in the nuclear/cytoskeletal fractions. Further, both presynaptic and postsynaptic markers (synaptophysin and PSD-95, respectively) were enriched in hippocampal synaptosome preparations compared to whole hippocampus. Additionally, partial depletion of astrocyte (GFAP) and microglia (Iba1) markers was demonstrated in the synaptosome-containing fractions, which contained lower levels of these protein markers than whole hippocampus and the nuclear/cytoskeletal fractions. This suggests the presence of a low degree of glia-derived material typical of synaptosomal preparations (Chicurel et al. 1993; Gylys et al. 2000; VanGuilder et al. 2010).

Transcriptomic Analysis of Cognitively Stratified Hippocampal Synaptosomes

Whole genome transcriptomic analysis [a subset of which is described in VanGuilder et al. (2011a)] was performed on hippocampal synaptosomal mRNA derived from the cognitively stratified animals to determine differences in gene expression between adult, aged intact, and aged impaired animals (n=5–7/group). Of the total 22,517 probes present on the microarray, genes corresponding to 10,630 probes were confidently detected. mRNAs corresponding to 1,414 probes demonstrated statistically significant differences between groups (adult, aged intact, and aged impaired, one-way ANOVA, $p<0.05$). A median FDR of 0.37 was calculated,

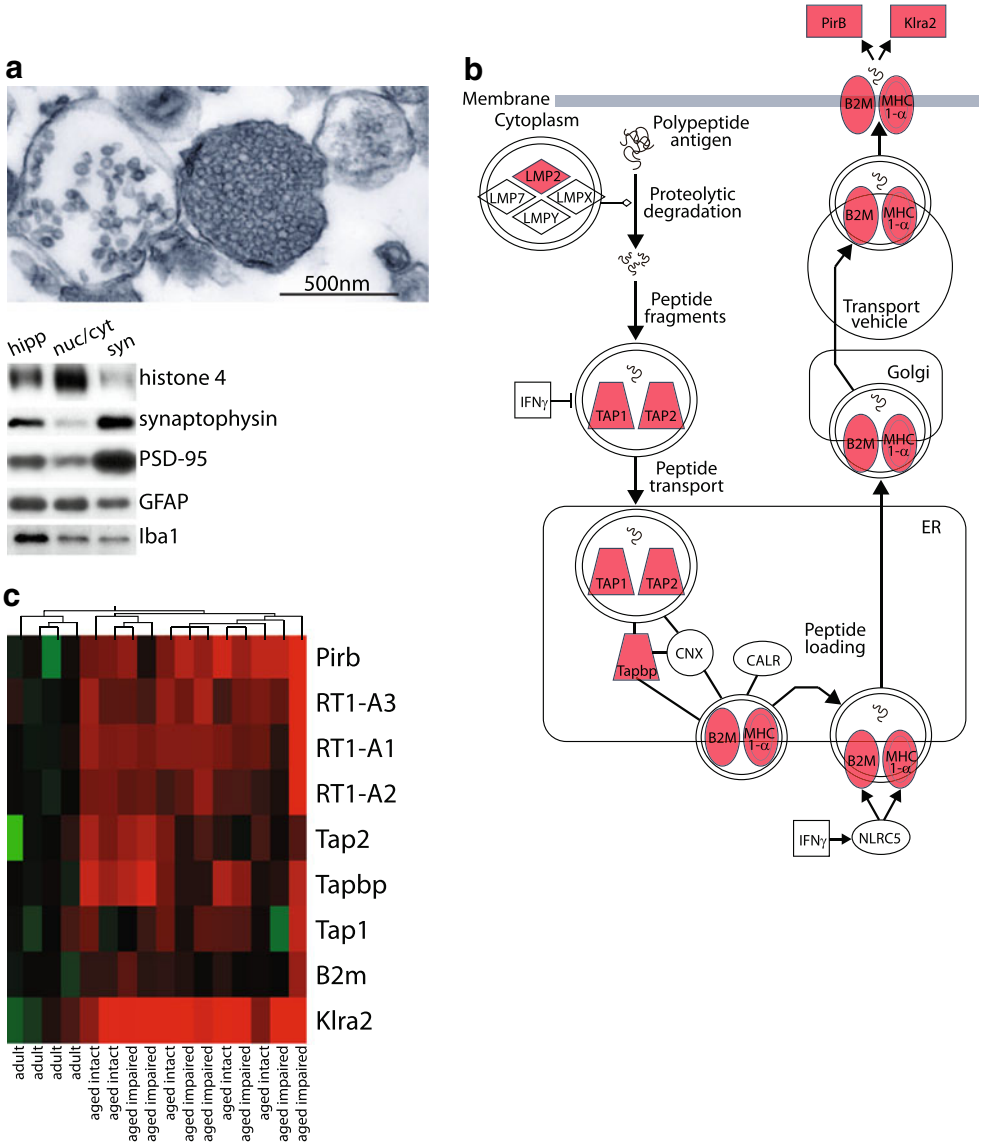

Fig. 1 Whole genome gene expression analysis of hippocampal synaptosomes. **a** Hippocampal synaptosome-containing fractions were evaluated by electron microscopy and immunoblotting to ensure enrichment of both presynaptic and postsynaptic elements and depletion of nuclear contaminants. Electron microscopic visualization of synaptosome preparations revealed intact synaptosomes with both vesicle-filled presynaptic compartments and postsynaptic terminals. Immunoblot assessment of whole hippocampal homogenate [hipp], nuclear/cytosolic combined fractions [nuc/cyt], and synaptosome fractions [syn] demonstrated depletion of the nuclear marker histone 4, enrichment of the presynaptic vesicle-associated protein synaptophysin and the postsynaptic scaffolding protein PSD-95, and moderate astrocytic GFAP and microglial Iba1 protein content. **b** MHCI expression values from the microarray analysis were overlayed on a MHCI pathway schematic (*red* increased in aged as compared to adult). **c** Expression of MHCI pathway components determined to be significantly regulated with aged are presented. Individual animals from adult, aged intact, and aged impaired groups (n=5–7/group) are presented (*red* increased; *green* decreased relative to mean adult)

which is similar to, but slightly higher than, previous examinations of hippocampal aging FDR = 0.23–0.29 (Rowe et al. 2007; Kadish et al. 2009; Blalock et al. 2010), likely due to the inclusion of EST probes and multiple probe sequences for some genes. One hundred eight mRNAs were significantly regulated with cognitive performance (aged intact vs. aged impaired), 781 demonstrated statistically significant differences specifically with aging (adult vs. aged intact), and 707 were regulated with both aging and cognitive status (adult vs. aged impaired) for a total of 1,002 differentially expressed mRNAs passing post hoc testing and fold change filter criteria.

GO analysis of the differentially expressed mRNAs identified "antigen processing and presentation of peptide antigen" ($p=2.82\times10^{-8}$, Fisher's exact test), "immune response" ($p=5.59\times10^{-5}$), and "MHC class I protein complex" ($p=0.02$) (Table 4) as the most highly regulated biological process

Table 4 Gene ontology analysis

GO ID #	GO accession #	GO term	*p* value
23156	GO:0048002	Antigen processing and presentation of peptide antigen	2.8×10^{-08}
11793	GO:0019882 GO:0030333	Antigen processing and presentation	2.5×10^{-08}
18603	GO:0042611	MHC protein complex	5.6×10^{-05}
4964	GO:0006955	Immune response	5.6×10^{-05}
18604	GO:0042612	MHC class I protein complex	2.0×10^{-02}

categories. Similarly, Ingenuity Pathway Analysis also identified the MHCI antigen presentation pathway, including three MHCI isoforms (RT1-A1, RT1-A2, and RT1-A3), B2m, Tapbp, Tap1, Tap2, and two MHCI receptors (PirB, Klra2), as upregulated with aging ($p=5.9\times10^{-5}$, Fisher's exact test). This MHCI pathway and upregulation of individual components are depicted in Fig. 1b. Synaptosomal expression of MHCI pathway components, as determined by transcriptomic profiling, is presented as a heatmap in Fig. 1c.

Confirmation of transcriptomic data was performed in whole hippocampus–synaptosome samples (cohort 1) and in unfractionated hippocampal subregions (CA1, CA3, DG; cohort 2) by qPCR analysis of MHCI pathway components including: MHCIαisoforms RT1-A1 (RT1 class Ia, locus A1), RT1-A2 (RT1 class Ia, locus A2), and RT1-A3 (RT1 class I, locus A3); MHCI cofactor beta-2 microglobulin (B2m); Tap1 (antigen processing genes transporter 1, ATP-binding cassette, subfamily B), Tap2 (transporter 2, ATP-binding cassette, subfamily B), and Tapbp (TAP binding protein); and the MHCI receptors PirB (paired immunoglobulin-like receptor B) and Klra2 (killer cell lectin-like receptor, subfamily A, member 2). qPCR data are summarized as ratios between group means in Table 5. Comparison of adult and aged rats confirmed increased expression of RT1-A1, RT1-A2, RT1-A3, Tap2, Tapbp, PirB, and Klra2 with aging in hippocampal synpatosomes (*t* test, BHMTC, $p<0.05$). In unfractionated hippocampal subregions, changes in mRNA expression were less pronounced with RT1-A1, RT1-A3, Tap2, and PirB significantly increased with aging in CA1, and RT1-A1, PirB, and Klra2 induced with aging in CA3. In this analysis, no significant differences with aging were observed in DG.

To identify potential cognitive status-associated changes in MHCI pathway gene expression, a three-group statistical comparison (adult, aged intact, and aged impaired) was also performed on expression of MHCI pathway genes by ANOVA with BHMTC and with SNK post hoc testing (Table 5). Age-related induction (aged intact vs. adult and aged impaired vs. adult) of most pathway components was evident in synaptosomal samples. Significant induction was also observed to a lesser degree in CA1 and CA3, while no significant changes were observed in DG. Cognition-specific induction of Tap1, Tapbp, and PirB were of a smaller magnitude and were limited to synaptosomal samples in the aged impaired vs. aged intact comparison.

Protein Level Expression of MHCI and PirB

To determine whether age-related mRNA level induction of the MHCI pathway is reflected at the level of protein expression, hippocampal synaptosomes and CA1, CA3, and DG subregion dissections were immunoblotted for MHCI and PirB. MHCI protein was detected and quantified using the pan-MHCI antibody Ox-18, which detects all three classical MHCI (RT1-A1, RT1-A2, RT1-A3) gene products. MHCI-immunoreactive bands were observed at 36 and 45 kDa, which have been suggested to reflect soluble and membrane-associated forms of MHCI, respectively (Zhai and Knechtle 1998). In synaptosomes, the 45-kDa MHCI-immunoreactive band was significantly increased in both aged intact (173±21.7 %, $p<0.05$, SNK) and aged impaired (162±11.9 %, $p<0.05$, SNK) rats compared to adults (Fig. 2). In subregion dissections, an age-related increase in both the 36- and 45-kDa bands (ranging from 17–89 %) was detected in CA1 and DG (Fig. 2). Additionally, CA1 expression of the 36-kDa MHCI form was higher (14 %) in the aged cognitively impaired than age-matched cognitively intact animals ($p<0.01$, SNK).

No differences in synaptosomal PirB protein content were observed (Fig. 3) with aging or cognitive status. However, PirB expression was elevated in aged, cognitively impaired rats compared to adults (SNK, $p<0.05$), with a similar trend in the aged cognitively intact group (Fig. 3), and when all aged animals were compared to adults, PirB protein was significantly increased (61 %, $p<0.05$, *p* value, *t* test). PirB expression in DG was increased by 57 % when all aged animals were compared to adults ($p<0.05$, *t* test). The three-group comparison of PirB protein expression in the DG approached significance (ANOVA, $p=0.06$).

Anatomical Localization of MHCI and PirB Protein Expression in the Rat Hippocampus

To identify the hippocampal distribution and cellular localization of MHCI and PirB, in the aged hippocampus, we

Table 5 qPCR analysis of gene expression

Gene	Aged vs. adult (ratio, *t* test *p* value)				Aged intact vs. adult (ratio, SNK *p* value)				Aged impaired vs. adult (ratio, SNK *p* value)				Aged impaired vs. aged intact (ratio, SNK *p* value)			
	Syn	CA1	CA3	DG	Syn	CA1	CA3	DG	Syn	CA1	CA3	DG	Syn	CA1	CA3	DG
RT1-A1	2.10#	1.56##	1.45##	–	1.88*	1.63*	1.51**	–	2.35*	1.51*	1.40*	–	–	–	–	–
RT1-A2	1.51###	–	–	–	1.46**	2.03*	–	–	1.57*	–	–	–	–	–	–	–
RT1-A3	1.92##	1.45###	–	–	–	1.43**	–	–	2.22**	1.47**	–	–	–	–	–	–
B2m	1.49##	–	–	–	1.48*	–	–	–	1.50*	–	–	–	–	–	–	–
Tap1	–	–	–	–	–	–	–	–	1.48*	–	–	–	1.49*	–	–	–
Tap2	1.59#	1.31##	–	–	–	1.35*	–	–	–	1.28*	–	–	–	–	–	–
Tapbp	1.32#	–	–	–	–	–	–	–	1.47*	–	–	–	1.27*	–	–	–
PirB	1.90#	1.79###	1.55##	–	–	1.89**	1.60*	–	2.50***	1.72**	1.49*	–	1.81**	–	–	–
Klra2	2.30#	–	1.91###	–	2.43*	–	1.93*	–	2.16*	–	1.90**	–	–	–	–	–

Age-based comparisons: two-tailed *t* test with BHMTC (#$p<0.05$; ##$p<0.01$; ###$p<0.001$); three-group data: one-way ANOVA/BHMTC with SNK post hoc (*$p<0.05$; **$p<0.01$; ***$p<0.001$). Data are presented as ratios of group means for the comparisons described in column headings (formatted as numerator vs. denominator). Values >1.0 indicate higher transcript levels in the groups used as numerators in the ratio comparisons

performed immunohistochemical analyses against pan-MHCI (Ox-18) and one of its more highly characterized receptors, PirB, using tissue samples from aged animals (26 months, cohort 3). MHCI immunoreactivity was apparent throughout the aged hippocampus, with cytosolic staining evident in the pyramidal cell and granule cell layers and diffuse staining in the neuropil, particularly in the *stratum lacunosum-moleculare* (Fig. 4a). There was also a region of diffuse MHCI expression in CA3, in close proximity to the pyramidal cell layer. Co-localization of MHCI and the microglia-specific marker Iba1 demonstrated cytosolic MHCI expression in microglial cell bodies and processes (Fig. 4b). No co-expression of MHCI with the astrocyte marker GFAP was observed (data not shown). Co-staining of MHCI and the dendrite-associated protein MAP2 (microtubule-associated protein 2) identified MHCI-immunoreactive glia with processes directly apposed to MAP2-immunoreactive dendritic processes (Fig. 4c). Lastly, punctate MHCI staining co-localized with PSD95-immunoreactive postsynaptic terminals of excitatory synapses (Fig. 4d). Unlike previous observations in the lateral geniculate nucleus (Datwani et al. 2009), co-localization of MHCI and the presynaptic vesicle protein synapsin 1 in hippocampus was not observed (data not shown).

The hippocampal distribution of PirB was also determined. Punctate PirB immunoreactivity was identified throughout the hippocampus, with concentrated expression in pyramidal cell layers of both CA1 and CA3 (Fig. 5a). An area of intense somatic PirB immunoreactivity, consistent with CA2 pyramidal cells (Lein et al. 2004), was apparent in all samples assessed. PirB was expressed throughout the hippocampus in neuronal axons and dendrites, as demonstrated by co-localization with heavy chain neurofilament (NFh; Fig. 5b) and MAP2 (Fig. 5d), respectively. Additionally, PirB was evident as perisomatic staining in large, NFh-expressing neurons in the pyramidal cell layer (Fig. 5c), with similar immunoreactivity observed surrounding MAP2-immunoreactive neuronal somata (Fig. 5d). A subset of pyramidal layer neurons with perisomatic PirB staining contained somatic/cytosolic MHCI immunoreactivity (Fig. 5e), as well as a degree of PirB/MHCI co-localization, indicating co-expression of MHCI and PirB by hippocampal neurons. No PirB was detected in Iba1^{+} or GFAP^{+} cells, indicating that microglia and astrocytes in the aged hippocampus do not express PirB. For each secondary antibody, a negative control was included, that was incubated with secondary antibody, but with primary antibodies excluded. No detectable fluorescent signals were observed on these controls by confocal microscopy (Fig. S1).

Discussion

To date, studies investigating potential molecular mechanisms of hippocampal aging indicate a highly complex

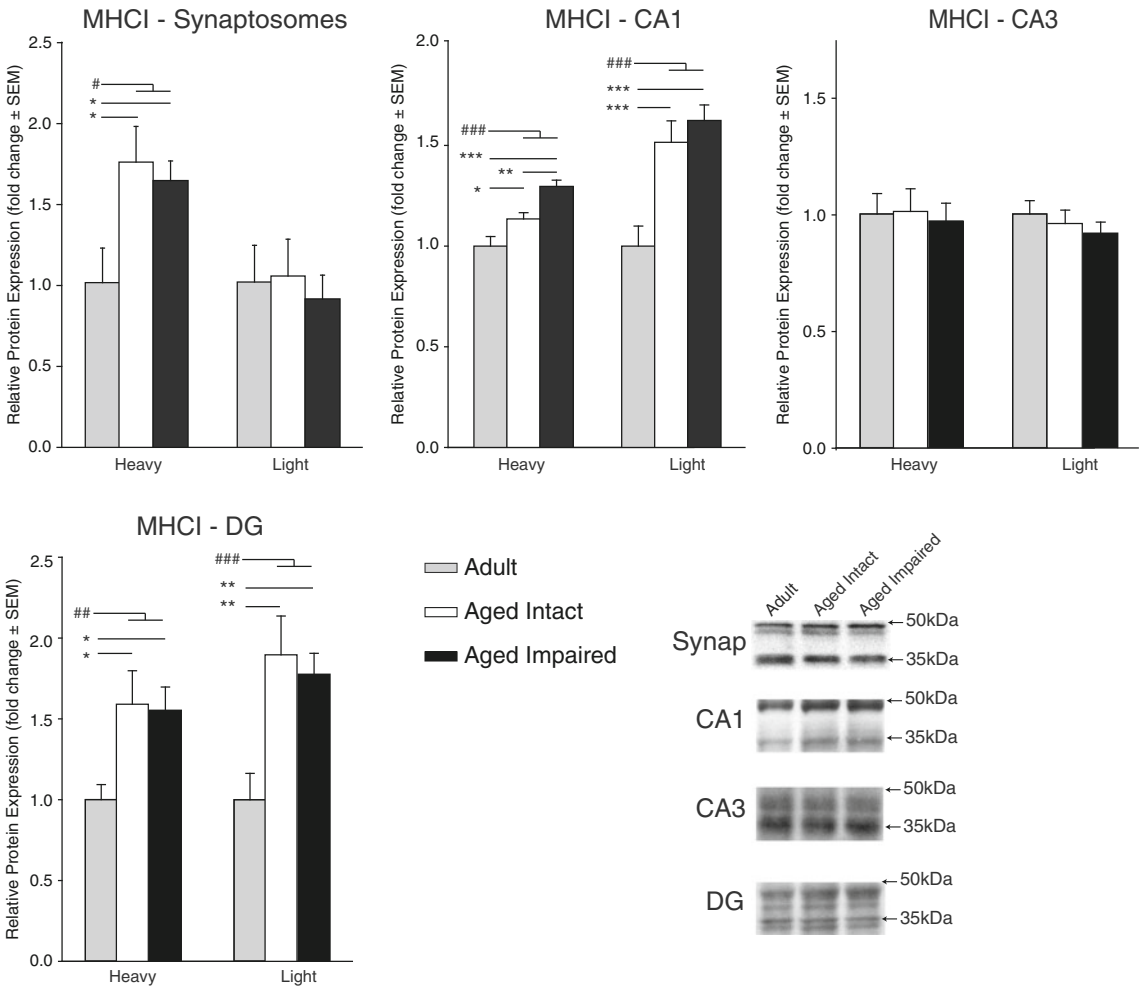

Fig. 2 Hippocampal MHCI protein expression with aging. MHCI protein expression in hippocampal synaptosomes and unfractionated CA1, CA3, and DG was assessed by immunoblotting with the pan-MHCI antibody (Ox-18). MHCI protein was detected in both the previously described heavy and light forms. Representative immunoblot examples are shown in *insets* (ANOVA, SNK: $^{*}p<0.05$, $^{**}p<0.01$, $^{***}p<0.001$; *t* test: $^{\#}p<0.05$, $^{\#\#\#}p<0.001$, n=5–7/group)

combination of alterations in metabolism, neurotransmission, oxidative stress, and neuroimmune activation (Barnes 1979; Berlett and Stadtman 1997; Barnes 2003; Lucin and Wyss-Coray 2009; Ownby 2010). Assessment of processes

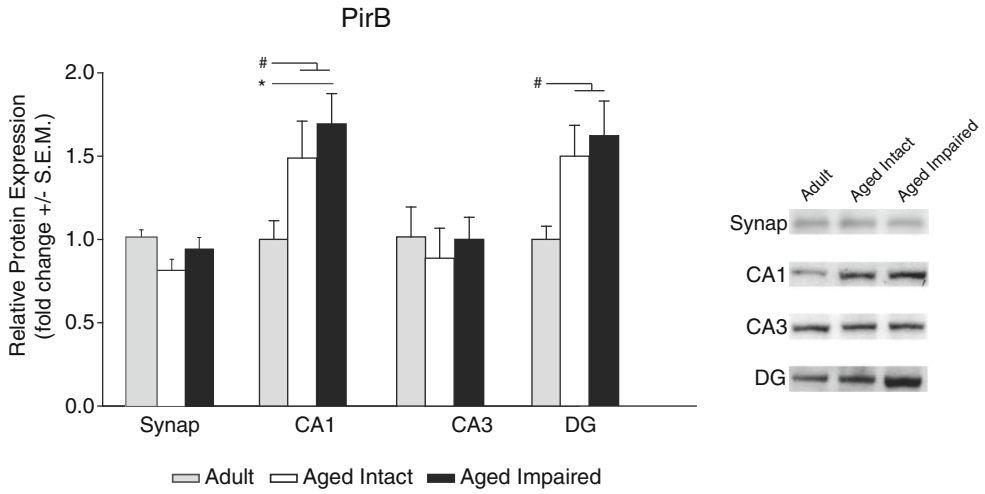

Fig. 3 Hippocampal PirB protein expression with aging. PirB protein expression in hippocampal synaptosomes and unfractionated CA1, CA3, and DG was assessed by immunoblotting. Representative immunoblot examples are shown in insets (ANOVA, SNK: $^{*}p<0.05$; *t* test: $\#p<0.05$, n=5–7/group)

dysregulated with aging, and their potential association to cognitive performance, provides insight into what is likely an additive array of insults that results in impaired neuronal function and ultimately impaired learning and memory (VanGuilder and Freeman 2011). To examine the effect of advanced aging on a neuroimmune signaling mechanism with reported roles in synapse regulation, as well as its potential role in age-related cognitive impairment, we evaluated hippocampal gene and protein expression of MHCI antigen processing and presentation pathway components and the PirB receptor in adult and aged rats behaviorally characterized by Morris water maze testing. Overexpression of the MHCI pathway was identified by bioinformatic analysis of genes differentially expressed with advanced aging in hippocampal synaptosomes. Additional processes and pathways were suggested to be regulated with increasing age, and a subset of differentially expressed genes was regulated specifically with cognitive impairment. Future studies will examine pathways, networks, and processes represented by cognitive decline-associated genes, assess potential correlation of genes/processes with spatial learning and memory impairment, and identify commonalities with previous studies [e.g., Rowe et al. (2007)].

This work is the first demonstration that advanced aging induces gene expression of the MHCI pathway in the hippocampus. Quantitative analysis of mRNA expression across multiple animal cohorts demonstrated a coordinated upregulation of multiple components of the MHCI pathway including classical MHC class I transcripts (RT1-A1, RT1-A2, RT1-3), the MHCI cofactor B2m, antigen processing machinery (Tap1, Tap2, Tapbp), and MHCI receptors (PirB, Klra2) with aging in hippocampal synaptosome preparations and dissected hippocampal subregions. Similarly, upregulation of MHCI mRNA was reflected at the level of total MHCI protein expression in both hippocampal synaptosome preparations and discrete hippocampal subregions. Protein expression of one known MHCI receptor, PirB, was also demonstrated to be elevated with aging in both cognitively intact and cognitively impaired aged rats.

The cellular and sub-cellular distribution of MHCI protein has not been previously described in the aged hippocampus. Similar to previous studies of other brain regions and cultured neurons (Streit et al. 1989; Goddard et al. 2007; Needleman et al. 2010), we identified cytosolic MHCI expression in hippocampal microglia, and also in hippocampal neurons. We have previously described both mild and moderate activation of microglia throughout the aged hippocampus (VanGuilder et al. 2011a), and future work will determine whether MHCI protein expression is associated with microglial activation, or occurs in "resting", non-activated microglia. We did not observe astrocytic MHCI protein expression in the aged hippocampus, although in vitro studies of cultured astrocytes suggest both constitutive (Massa et al. 1993) and inducible [e.g., by interferon gamma (Jarosinski and Massa 2002) and tumor necrosis factor (Lavi et al. 1988)] expression of MHCI. It is possible that astrocytes in the aged hippocampus express small amounts of MHCI protein at levels below the threshold of immunohistochemical detection, or that MHCI protein is not expressed by astrocytes without stimuli such as cytokines or infection.

Enrichment of MHCI transcripts has been demonstrated in the dendritic *stratum radiatum* compared to cell-body containing *stratum pyramidale* in rat hippocampal CA1 (Zhong et al. 2006), suggesting a preferential localization of MHCI mRNAs in distal neuronal processes. In agreement with these findings, we identified MHCI expression in excitatory postsynaptic densities, demonstrated by co-localization with PSD-95. MHCI has been localized to both pre- and postsynaptic compartments in the cortex (Datwani et al. 2009; Needleman et al. 2010), but the localization of MHCI at hippocampal excitatory postsynaptic densities has not been previously reported. Interestingly, we did not observe presynaptic expression of hippocampal MHCI, as assessed by co-localization with synapsin I. Further characterization studies similar to those performed in the visual cortex (Needleman et al. 2010) are needed to fully map the cellular and neuronal expression, and the subcellular localization, of specific MHCI proteins in the hippocampus.

In our studies, transcript level expression of specific classical MHCI genes (RT1-A1, RT1-A2, RT1-A3) was consistently induced with aging in hippocampal synapses and across multiple hippocampal subregions. Affinity reagents for examining rat MHCI protein, however, are currently limited. Using a pan-MHCI antibody, which recognizes all three classical gene products, we observed age-related induction of both a light and heavy form of MHCI, which have been suggested to represent soluble and membrane-associated forms, respectively (Zhai and Knechtle 1998). Additional studies are needed to quantify specific classical MHCI proteins, and mass spectrometry approaches, rather than antibodies, will most likely be necessary due to the high homology between these proteins. Differences in the specificity of reagents currently available for quantitation of MHCI at the gene (isoform-specific primers/probes) and protein (pan-MHCI antibodies) levels may underlie dissimilarities between MHCI mRNA and protein quantitation (e.g., in DG) observed in the present studies. Additionally, the stability and translation of MHCI transcripts and degradation of MHCI proteins in the aged hippocampus remains to be characterized and may contribute to the observed variance between mRNA and protein levels.

The regulation and function of MHCI has been most fully examined in the adaptive immune system where MHCI presents intracellular peptides to CD8+ cytotoxic T cells (Lawlor et al. 1990). MHCI genes are divided into classical and non-classical groups with classical MHCIs (including

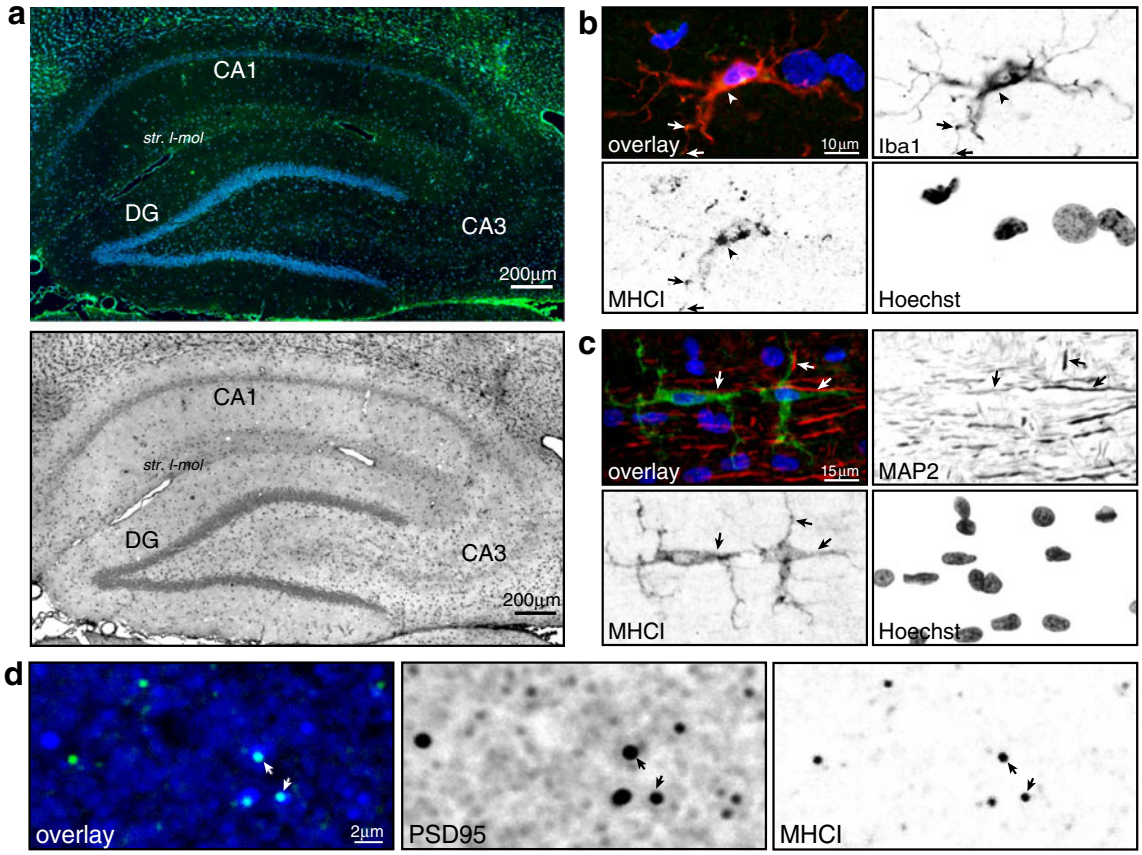

Fig. 4 Cellular localization of MHCI expression in aged rat hippocampus. To identify the hippocampal subregions and cell types expressing MHCI at the protein level, immunohistochemical co-localization experiments were conducted using MHCI (Ox-18) paired with cell-specific antibody markers. **a** Broad-field visualization of MHCI immunoreactivity demonstrated MHCI expression distributed throughout the hippocampal formation with punctate, putatively synaptic staining concentrated in *stratum lacunosum-moleculare* (*str. l-mol*) and cytosolic staining in cell body-containing layers in all three subregions of interest (CA1, CA3, DG), with notably higher expression in the CA2/3 pyramidal cell layer (*green* MHCI, *blue* Hoechst). MHCI immunohistochemistry is also presented in inverted grayscale for enhanced contrast visualization of MHCI immunoreactivity in *stratum lacunosum-moleculare*. **b** MHCI immunoreactivity was co-localized with Iba1, a microglia-specific calcium binding protein, with staining evident in both microglial cell bodies (*arrowhead*) and processes (*arrows*). MHCI co-localization with Iba1 was evident in morphologically normative microglia, suggesting a basal level of MHCI protein expression in hippocampal microglia. *Red* Iba1, *green* MHCI, *blue* Hoechst, *orange* Iba1/MHCI co-localization. **c** A subset of MHCI-immunoreactive glial cells, including both somata and projections, was directly apposed to MAP2-expressing dendrites (*arrows*). *Red* MAP2, *green* MHCI, *blue* Hoechst. **d** Co-localization of PSD95 and MHCI immunoreactivity (*arrows*) demonstrated that MHCI protein is expressed in PSD95-positive, likely excitatory, postsynaptic terminals. *Blue* PSD95, *green* MHCI, *cyan* PSD95/MHCI co-localization

the rat RT1-A1, RT1-A2, and RT1-A3 genes described here) ubiquitously expressed across tissues and cell types including neurons (Bjorkman and Parham 1990). Processing of mature MHCI protein occurs in the endoplasmic reticulum (ER) where it binds B2m and associates with Tapbp and the Tap complex (Tap1 and Tap2). Proteosomal degradation products of endogenous or intracellular viral proteins are shuttled across the ER membrane into the lumen through the Tap complex and loaded onto MHCI (Rufer et al. 2007). The mature MHCI complex (MHCI, B2m, and antigen) translocates to the cell surface, where it presents antigens to a variety of receptors including CD3-containing receptors, the paired immunoglobulin-like receptors (Pir), and natural killer cell lectin-like receptor (Klra2) (Takai 2005; Zohar et al. 2008). The regulation and function of MHCI in the central nervous system is much less well understood, though there is an increasing interest in how MHCI may regulate synaptic function and structure (Boulanger 2009).

The age-related induction of MHCI and other MHCI pathway components described here may have important functional consequences, as recent evidence has illuminated the role of MHCI in the formation and plasticity of synaptic connections [for review, see Shatz (2009) and Fourgeaud and Boulanger (2010)]. MHCI is required for synapse elimination during development of ocular dominance in the lateral geniculate nucleus, as demonstrated through blockade of all MHCI signaling in both B2m$^{-/-}$ and B2m$^{-/-}$/Tap1$^{-/-}$ knockout mice (Huh et al. 2000), and in mice with

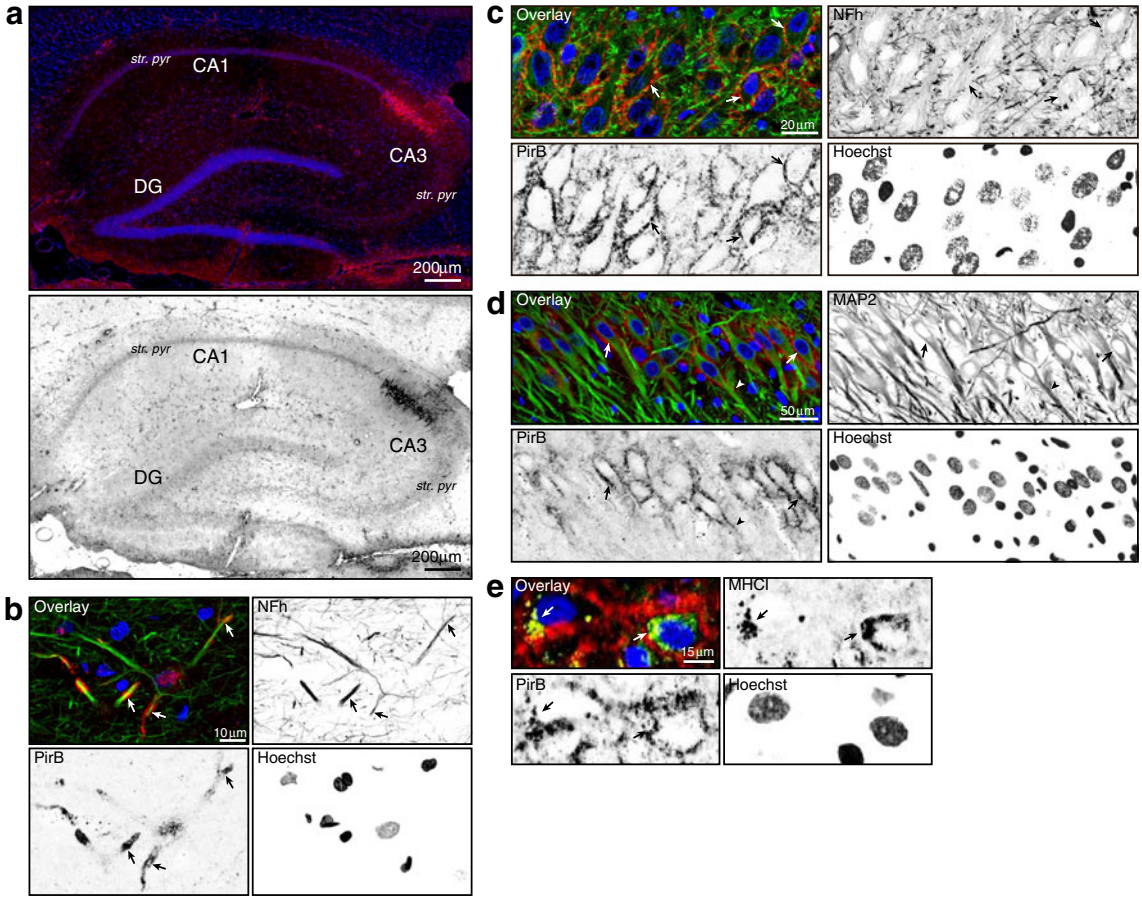

Fig. 5 Hippocampal expression of PirB. Distribution of hippocampal PirB protein expression was assessed by immunohistochemical co-localization with cell-specific markers. **a** PirB immunoreactivity (*magenta*) was evident throughout the aged hippocampus as diffuse, punctate staining, with greater expression in *stratum pyramidale* (*str. pyr*) of both CA1 and CA3. Additionally, intense somatic PirB immunoreactivity was apparent in CA2 pyramidal cells. PirB immunohistochemistry is also depicted in inverted grayscale for enhanced contrast. **b** Co-localization of PirB and heavy neurofilament (*NFh*) immunoreactivity demonstrated axonal expression of PirB in hippocampal neurons (*arrows*). *Green* NFh, *red* PirB, *blue* Hoechst, *yellow* PirB/NFh co-localization. **c** Perisomatic PirB expression in CA3 pyramidal cells, as demonstrated by perisomatic PirB immunoreactivity surrounding NFh-containing pyramidal cell somata (*arrows*). *Green* NFh, *red* PirB, *blue* Hoechst, *yellow* PirB/NFh co-localization. **d** Perisomatic PirB immunoreactivity was evident in a subset of large MAP-2-immunoreactive neurons (*arrows*) and proximal dendrite segments (*arrowhead*). *Green* MAP2, *red* PirB, *blue* Hoechst. **e** Pyramidal neurons with perisomatic PirB staining contained cytoplasmic MHCI immunoreactivity (*arrows*), demonstrating neuronal co-expression of MHCI and one of its receptors, PirB. *Green* MHCI, *red* PirB, *blue* Hoechst, *yellow* MHCI/PirB co-expression

deletion of two specific classical MHCI genes ($H2K^{d-/-}$, $H2D^{b-/-}$) (Datwani et al. 2009). Additionally, the number of cortical synapses is increased in $B2m^{-/-}$ mice throughout development (Glynn et al. 2011). Inversely, overexpression of neuronal MHCI ($H2K^b$) decreases both GABAergic and glutamatergic synaptic density of cultured neurons in vitro (Glynn et al. 2011). Similarly, increased neuronal overexpression of the MHCI gene $H2D^b$ inhibits neurite outgrowth in vitro (Washburn et al. 2011) and decreases hippocampal GAP-43 and synaptophysin staining in vivo, which has been interpreted as indicating a loss of presynaptic terminals (Wu et al. 2011). Functionally, blockade of surface MHCI (through $B2m^{-/-}$ or $B2m^{-/-}/Tap1^{-/-}$) enhances hippocampal excitatory postsynaptic potentials (Huh et al. 2000) and currents (Goddard et al. 2007). In cortical cultures, increased MHCI suppresses the frequency and amplitude of excitatory postsynaptic currents while blockade of cell surface MHCI increases both measures (Glynn et al. 2011). Similarly, in slice preparations, inhibition of cell surface MHCI increases NMDAR-mediated currents (Fourgeaud et al. 2010). Together, these reports suggest that altered neuronal MHCI expression may have important functional consequences in the aging nervous system.

In light of these findings, the age-related increase in MHCI expression that we observed, combined with our detection of MHCI in synaptic postsynaptic densities, may leave synapses susceptible to increased LTD and decreased excitatory synapse density, both of which are characteristic of the aged hippocampus. Physiologically, the aged hippocampus demonstrates a significant deficiency in the ability

to initiate and maintain LTP and is highly susceptible to LTD (Norris et al. 1996; Barnes 2003). Additionally, alterations in dendritic branching and spine density (Hedden and Gabrieli 2004; Burke and Barnes 2006), decreases in hippocampal NMDA and AMPA receptor expression (Sonntag et al. 2000), dysregulation of glutamatergic neurotransmission (Auer 1991) occur with aging. Instability of hippocampal LTP in aged rats is associated with poor cognitive performance in spatial tasks of hippocampus-dependent learning and memory (Barnes 1979) and preferential loss of perforated axospinous synapses, which are implicated in high-efficiency synaptic transmission (Geinisman et al. 1986). Previously reported improvements in rotarod task learning and retention in $H2K^{d-/-}/H2D^{b-/-}$ mice (McConnell et al. 2009) provide support for future investigations identifying the physiological and behavioral outcomes of increased MHCI expression in aged rats.

MHCI has a number of receptors in the peripheral immune system (Lanier 1998; Long 1999), but the receptors for MHCI in the brain are only beginning to be characterized. In this study, we identified and confirmed age-related regulation of two known MHCI receptors PirB (Takai 2005) and Klra2 (also known as Ly49) (Zohar et al. 2008). Further characterization demonstrated increased PirB protein in CA1 with both aging and cognitive decline. While the PirB mRNA and protein data from CA1 was highly concordant, the mRNA changes observed in synaptosomes and CA3 were not recapitulated at the protein level. The existing knowledge on PirB regulation in neurons is extremely limited, and additional studies are needed to determine whether the discordance in protein vs. mRNA expression data is a result of regulation of protein expression through alternative mechanisms, or differential localization or protein transport. The roles of PirB in the brain are largely undetermined, but knockout of functional PirB expression has been demonstrated to enhance ocular dominance plasticity in the visual cortex during development and throughout adulthood (Syken et al. 2006). Detailed PirB protein localization in the hippocampus has not been previously reported and our results demonstrate axonal and perisomatic PirB expression in neurons with no immunoreactivity evident in astrocytes or microglia. Interestingly, a population of pyramidal layer neurons was found to express both perisomatic PirB and somatic MHCI. Signaling of MHCI to PirB in the brain has not yet been demonstrated, and future in vivo studies determining the functional receptors for MHCI are required to identify the signaling mechanisms of neuroglial MHCI.

Recently, PirB has also been identified as a receptor for the myelin-associated factors Nogo-A (neurite outgrowth inhibitor A), MAG (myelin-associated glycoprotein), and OMgp (oligodendrocyte myelin glycoprotein) (Atwal et al. 2008) in addition to MHCI. Increased binding of myelin-derived factors to PirB produces alterations in F-actin polymerization, thus influencing local synaptic architecture and plasticity (Zagrebelsky et al. 2010; Llorens et al. 2011). We have previously observed cognitive impairment-specific upregulation of Nogo-A, MAG, and OMgp at the level of protein, but not mRNA, in hippocampal synaptosomes and subregions derived from the same rat cohorts presented in this study (VanGuilder et al. 2011b, 2012). It is possible that myelin-associated factors induced with cognitive impairment may act, in part, through PirB to contribute to age-related deficits of hippocampal function.

The data presented here demonstrate coordinated upregulation of the MHCI pathway expression with hippocampal aging. Induction of MHCI with aging has been demonstrated in peripheral motor neurons (Edstrom et al. 2004), but little is known about the effects of advanced aging on MHCI expression in the central nervous system. In agreement with our findings, however, meta-analysis of primary hippocampal microarray data from aging studies (Berchtold et al. 2008; Kadish et al. 2009; Blalock et al. 2010; Zeier et al. 2011) reveals age-related induction of MHCI pathway components across species, in rodent, non-human primate, and human hippocampus; however, specific analysis of the MHCI pathway has not been previously performed. With the growing understanding of the functional pleiotropy (Radisky et al. 2009) of MHCI and PirB, which serve both canonical roles in immune response and recently identified roles in regulating synaptic transmission and connectivity (Shatz 2009; Fourgeaud and Boulanger 2010), induction of this pathway may contribute to the physiological and morphological changes characteristic of brain aging and hippocampal dysfunction, including alterations in electrophysiological correlates of plasticity and synapse density. Future gain- and loss-of-function studies examining MHCI and PirB signaling are needed to elucidate the potential impact of this signaling mechanism on hippocampal dysfunction with brain aging.

Acknowledgments This work was supported by funding from the National Institute on Aging, National Institutes of Health (5R01AG026607, 1F31AG038285), and Donald W. Reynolds Foundation. The authors wish to thank the Penn State College of Medicine Genome Sciences and Imaging Facilities and Robert Brucklacher for technical assistance and Wayne Jarvis for assistance with figure creation.

Conflict of interest The authors have no conflicts of interest to declare.

References

Atwal JK, Pinkston-Gosse J, Syken J (2008) PirB is a functional receptor for myelin inhibitors of axonal regeneration. Science 322:967–970

Auer RN (1991) Excitotoxic mechanisms, and age-related susceptibility to brain damage in ischemia, hypoglycemia and toxic mussel poisoning. Neurotoxicology 12:541–546

Barnes CA (1979) Memory deficits associated with senescence: a neurophysiological and behavioral study in the rat. J Comp Physiol Psychol 93:74–104

Barnes CA (2003) Long-term potentiation and the ageing brain. Philos Trans R Soc Lond B Biol Sci 358:765–772

Benjamini Y, Drai D, Elmer G, Kafkafi N, Golani I (2001) Controlling the false discovery rate in behavior genetics research. Behav Brain Res 125:279–284

Berchtold NC, Cribbs DH, Coleman PD et al (2008) Gene expression changes in the course of normal brain aging are sexually dimorphic. Proc Natl Acad Sci USA 105:15605–15610

Berlett BS, Stadtman ER (1997) Protein oxidation in aging, disease, and oxidative stress. J Biol Chem 272:20313–20316

Bjorkman PJ, Parham P (1990) Structure, function, and diversity of class I major histocompatibility complex molecules. Annu Rev Biochem 59:253–288

Blalock EM, Grondin R, Chen KC et al (2010) Aging-related gene expression in hippocampus proper compared with dentate gyrus is selectively associated with metabolic syndrome variables in rhesus monkeys. J Neurosci 30:6058–6071

Boulanger LM (2009) Immune proteins in brain development and synaptic plasticity. Neuron 64:93–109

Burke SN, Barnes CA (2006) Neural plasticity in the ageing brain. Nat Rev Neurosci 7:30–40

Chicurel ME, Terrian DM, Potter H (1993) mRNA at the synapse: analysis of a synaptosomal preparation enriched in hippocampal dendritic spines. J Neurosci 13:4054–4063

Datwani A, McConnell MJ, Kanold PO et al (2009) Classical MHCI molecules regulate retinogeniculate refinement and limit ocular dominance plasticity. Neuron 64:463–470

Edstrom E, Kullberg S, Ming Y, Zheng H, Ulfhake B (2004) MHC class I, beta2 microglobulin, and the INF-gamma receptor are upregulated in aged motoneurons. J Neurosci Res 78:892–900

Fiocco AJ, Yaffe K (2010) Defining successful aging: the importance of including cognitive function over time. Arch Neurol 67:876–880

Fourgeaud L, Boulanger LM (2010) Role of immune molecules in the establishment and plasticity of glutamatergic synapses. Eur J Neurosci 32:207–217

Fourgeaud L, Davenport CM, Tyler CM, Cheng TT, Spencer MB, Boulanger LM (2010) MHC class I modulates NMDA receptor function and AMPA receptor trafficking. Proc Natl Acad Sci USA 107:22278–22283

Gavilan MP, Revilla E, Pintado C et al (2007) Molecular and cellular characterization of the age-related neuroinflammatory processes occurring in normal rat hippocampus: potential relation with the loss of somatostatin GABAergic neurons. J Neurochem 103:984–996

Geinisman Y, de Toledo-Morrell L, Morrell F (1986) Loss of perforated synapses in the dentate gyrus: morphological substrate of memory deficit in aged rats. Proc Natl Acad Sci USA 83:3027–3031

Glynn MW, Elmer BM, Garay PA et al (2011) MHCI negatively regulates synapse density during the establishment of cortical connections. Nat Neurosci 14:442–451

Goddard CA, Butts DA, Shatz CJ (2007) Regulation of CNS synapses by neuronal MHC class I. Proc Natl Acad Sci USA 104:6828–6833

Gylys KH, Fein JA, Cole GM (2000) Quantitative characterization of crude synaptosomal fraction (P-2) components by flow cytometry. J Neurosci Res 61:186–192

Hara Y, Park CS, Janssen WG, Punsoni M, Rapp PR, Morrison JH (2011) Synaptic characteristics of dentate gyrus axonal boutons and their relationships with aging, menopause, and memory in female rhesus monkeys. J Neurosci 31:7737–7744

Hedden T, Gabrieli JD (2004) Insights into the ageing mind: a view from cognitive neuroscience. Nat Rev Neurosci 5:87–96

Huh GS, Boulanger LM, Du H, Riquelme PA, Brotz TM, Shatz CJ (2000) Functional requirement for class I MHC in CNS development and plasticity. Science 290:2155–2159

Jarosinski KW, Massa PT (2002) Interferon regulatory factor-1 is required for interferon-gamma-induced MHC class I genes in astrocytes. J Neuroimmunol 122:74–84

Kadish I, Thibault O, Blalock EM et al (2009) Hippocampal and cognitive aging across the lifespan: a bioenergetic shift precedes and increased cholesterol trafficking parallels memory impairment. J Neurosci 29:1805–1816

Lanier LL (1998) NK cell receptors. Annu Rev Immunol 16:359–393

Lavi E, Suzumura A, Murasko DM, Murray EM, Silberberg DH, Weiss SR (1988) Tumor necrosis factor induces expression of MHC class I antigens on mouse astrocytes. J Neuroimmunol 18:245–253

Lawlor DA, Zemmour J, Ennis PD, Parham P (1990) Evolution of class-I MHC genes and proteins: from natural selection to thymic selection. Annu Rev Immunol 8:23–63

Lein ES, Zhao X, Gage FH (2004) Defining a molecular atlas of the hippocampus using DNA microarrays and high-throughput in situ hybridization. J Neurosci 24:3879–3889

Llorens F, Gil V, del Rio JA (2011) Emerging functions of myelin-associated proteins during development, neuronal plasticity, and neurodegeneration. FASEB J 25:463–475

Long EO (1999) Regulation of immune responses through inhibitory receptors. Annu Rev Immunol 17:875–904

Long LH, Liu RL, Wang F et al (2009) Age-related synaptic changes in the CA1 stratum radiatum and spatial learning impairment in rats. Clin Exp Pharmacol Physiol 36:675–681

Lucin KM, Wyss-Coray T (2009) Immune activation in brain aging and neurodegeneration: too much or too little? Neuron 64:110–122

Massa PT, Ozato K, McFarlin DE (1993) Cell type-specific regulation of major histocompatibility complex (MHC) class I gene expression in astrocytes, oligodendrocytes, and neurons. Glia 8:201–207

McConnell MJ, Huang YH, Datwani A, Shatz CJ (2009) H2-K(b) and H2-D(b) regulate cerebellar long-term depression and limit motor learning. Proc Natl Acad Sci USA 106:6784–6789

Narum SR (2006) Beyond Bonferroni: less conservative analyses for conservation genetics. Conservation Genetics 7:783–787

Needleman LA, Liu XB, El-Sabeawy F, Jones EG, McAllister AK (2010) MHC class I molecules are present both pre- and postsynaptically in the visual cortex during postnatal development and in adulthood. Proc Natl Acad Sci USA 107:16999–17004

Norris CM, Korol DL, Foster TC (1996) Increased susceptibility to induction of long-term depression and long-term potentiation reversal during aging. J Neurosci 16:5382–5392

Ogura K, Ogawa M, Yoshida M (1994) Effects of ageing on microglia in the normal rat brain: immunohistochemical observations. Neuroreport 5:1224–1226

Ownby RL (2010) Neuroinflammation and cognitive aging. Curr Psychiatry Rep 12:39–45

Paolicelli RC, Bolasco G, Pagani F et al (2011) Synaptic pruning by microglia is necessary for normal brain development. Science 333:1456–1458

Radisky DC, Stallings-Mann M, Hirai Y, Bissell MJ (2009) Single proteins might have dual but related functions in intracellular and extracellular microenvironments. Nat Rev Mol Cell Biol 10:228–234

Roumier A, Bechade C, Poncer JC et al (2004) Impaired synaptic function in the microglial KARAP/DAP12-deficient mouse. J Neurosci 24:11421–11428

Rowe WB, Blalock EM, Chen KC et al (2007) Hippocampal expression analyses reveal selective association of immediate-early, neuroenergetic, and myelinogenic pathways with cognitive impairment in aged rats. J Neurosci 27:3098–3110

Rufer E, Leonhardt RM, Knittler MR (2007) Molecular architecture of the TAP-associated MHC class I peptide-loading complex. J Immunol 179:5717–5727

Shamy JL, Buonocore MH, Makaron LM, Amaral DG, Barnes CA, Rapp PR (2006) Hippocampal volume is preserved and fails to predict recognition memory impairment in aged rhesus monkeys (*Macaca mulatta*). Neurobiol Aging 27:405–1415

Shatz CJ (2009) MHC class I: an unexpected role in neuronal plasticity. Neuron 64:40–45

Shi L, Linville MC, Tucker W, Sonntag WE, Brunso-Bechtold JK (2005) Differential effects of aging and insulin-like growth factor-1 on synapses in CA1 of rat hippocampus. Cereb Cortex 15:571–577

Small GW (2002) What we need to know about age related memory loss. BMJ 324:1502–1505

Sonntag WE, Bennett SA, Khan AS et al (2000) Age and insulin-like growth factor-1 modulate N-methyl-D-aspartate receptor subtype expression in rats. Brain Res Bull 51:331–338

Streit WJ, Graeber MB, Kreutzberg GW (1989) Peripheral nerve lesion produces increased levels of major histocompatibility complex antigens in the central nervous system. J Neuroimmunol 21:117–123

Syken J, Grandpre T, Kanold PO, Shatz CJ (2006) PirB restricts ocular-dominance plasticity in visual cortex. Science 313:1795–1800

Takai T (2005) Paired immunoglobulin-like receptors and their MHC class I recognition. Immunology 115:433–440

Tomaszewski FS, Cahn-Weiner DA, Harvey DJ et al (2009) Longitudinal changes in memory and executive functioning are associated with longitudinal change in instrumental activities of daily living in older adults. Clin Neuropsychol 23:446–461

VanGuilder HD, Bixler GV, Brucklacher RM et al (2011a) Concurrent hippocampal induction of MHC II pathway components and glial activation with advanced aging is not correlated with cognitive impairment. J Neuroinflammation 8:138

VanGuilder HD, Bixler GV, Sonntag WE, Freeman WM (2012) Hippocampal expression of myelin-associated inhibitors is induced with age-related cognitive decline and correlates with deficits of spatial learning and memory. J Neurochem 121:77–98

VanGuilder HD, Farley JA, Yan H et al (2011b) Hippocampal dysregulation of synaptic plasticity-associated proteins with age-related cognitive decline. Neurobiol Dis 43:201–212

VanGuilder HD, Freeman WM (2011) The hippocampal neuroproteome with aging and cognitive decline: past progress and future directions. Front Aging Neurosci 3:8–21

VanGuilder HD, Yan H, Farley JA, Sonntag WE, Freeman WM (2010) Aging alters the expression of neurotransmission-regulating proteins in the hippocampal synaptoproteome. J Neurochem 113:1577–1588

Washburn LR, Zekzer D, Eitan S et al (2011) A potential role for shed soluble major histocompatibility class I molecules as modulators of neurite outgrowth. PLoS One 6:e18439

Wu ZP, Washburn L, Bilousova TV et al (2011) Enhanced neuronal expression of major histocompatibility complex class I leads to aberrations in neurodevelopment and neurorepair. J Neuroimmunol 232:8–16

Yirmiya R, Goshen I (2011) Immune modulation of learning, memory, neural plasticity and neurogenesis. Brain Behav Immun 25:181–213

Zagrebelsky M, Schweigreiter R, Bandtlow CE, Schwab ME, Korte M (2010) Nogo-A stabilizes the architecture of hippocampal neurons. J Neurosci 30:13220–13234

Zeier Z, Madorsky I, Xu Y, Ogle WO, Notterpek L, Foster TC (2011) Gene expression in the hippocampus: regionally specific effects of aging and caloric restriction. Mech Ageing Dev 132:8–19

Zhai Y, Knechtle S (1998) Two distinct forms of soluble MHC class I molecules synthesized by different mechanisms in normal rat cells in vitro. Hum Immunol 59:404–414

Zhong J, Zhang T, Bloch LM (2006) Dendritic mRNAs encode diversified functionalities in hippocampal pyramidal neurons. BMC Neurosci 7:17

Zohar O, Reiter Y, Bennink JR et al (2008) Cutting edge: MHC class I–Ly49 interaction regulates neuronal function. J Immunol 180:6447–6451